ЖЭТФ, 2002, том 122, вып. 4 (10), стр. 746–764

SEMICLASSICAL APPROACH TO STATES NEAR THE POTENTIAL BARRIER TOP

V. A. Benderskii

Institute for Problems of Chemical Physics, Russian Academy of Sciences
142432, Moscow Region, Chernogolovka, Russia

Lab. Spectrometrie Physique, UJF
BP 87, St. Martin d'Heres, Cedex, France

E. V. Vetoshkin

Institute for Problems of Chemical Physics, Russian Academy of Sciences
142432, Moscow Region, Chernogolovka, Russia

E. I. Kats*

Institute Laue-Langevin
F-38042, Grenoble, France

Landau Institute for Theoretical Physics, Russian Academy of Sciences
142432, Chernogolovka, Moscow Region, Russia

Submitted 30 May 2002

Within the framework of the instanton approach, we present analytical results for the following model problems: (i) particle penetration through a parabolic potential barrier, where the instanton solution practically coincides with the exact (quantum) one; (ii) descriptions of highly excited states in anharmonic potentials of two types: double-well X^4 and decay X^3. For the former potential, the instanton method accurately reproduces not only single-well and double-well quantization, but also a crossover region (in contrast to the standard WKB approach that fails to describe the crossover behavior); for the latter potential, the instanton method allows studying the resonance broadening and collapse phenomena. We also investigate resonance tunneling that plays a relevant role in many semiconducting devices. We show that the instanton approach gives exact (quantum) results in a broad range of energies. Applications of the method and of the results are applicable to various systems in physics, chemistry, and biology exhibiting double-level behavior and resonance tunneling.

PACS: 05.45.-a, 05.45.Gg

1. INTRODUCTION

Semiclassical mechanics has a long history. Surprisingly, however, some long-standing problems still exist in the theory. One of them — the description of states near a potential barrier top with a sufficient accuracy — is the subject of this paper. It is known that the commonly used WKB method (phase integral approach) [1, 2] amounts to matching the wave functions for the classically allowed and forbidden regions. Technically, the procedure works for linear (or first-order) turning points and can be relatively simply performed only in one-dimensional problems. But one-dimensional problems are not of great physical importance, not only because the reduced dimensionality does not allow modelling many relevant experimental situations, but also (at least partially) because one-dimensional quantum mechanical problems can be rather easily solved numerically. Unfortunately, efficiency and accuracy of direct numerical methods in quantum mechanics rapidly degrade for multidimensional systems possessing many degrees of freedom because of an extraordinary amount of computational

*E-mail: kats@ill.fr

work required for calculations. Furthermore, an extention of the WKB procedure to multidimensional systems encounters fundamental difficulties because of the still unsolved matching problem for multidimensional WKB solutions, which become singular on caustic lines separating manifolds in phase space with real and imaginary momenta for each among N coordinates. Because the number of these domains increases as $N!$, it is a tremendous task for $N > 2$. After several decades of efforts, a complete and unifying descriptions of multidimensional WKB solutions is still unavailable.

The problem was first addressed long ago, and some attempts to overcome the difficulties of the WKB approach and to improve the accuracy of the method have been performed quite successfully. We note, e.g., [3], where the authors additionally included trajectories of a special type on the complex phase plane into the standard WKB method; the semiclassical motion along these trajectories is described by the Weber functions (also see [4]). But the choice of these additional special trajectories (which must be included in order to improve the accuracy of the WKB method near the barrier top) depends on the detailed form of the potential far from the top, and in each particular case, a nonuniversal procedure must therefore be performed from the very beginning (also see more recent publications [5], where the authors use some distortion of Stokes diagrams, or [6], where time-dependent quantum mechanical calculations for anharmonic and double-well oscillators have been performed).

Evidently, therefore, there is some need for a semiclassical approach different from the WKB method. One of the alternatives to the WKB semiclassical formalism, the so-called extreme tunneling trajectory, or instanton [7–9], could be very effective in calculating a globally uniform wave function of the ground state (i.e., a wave function without singularities). It allows finding semiclassical wave functions for a very broad class of potentials with arbitrary combinations of the first- and the second-order turning points. The method was recently adapted for the description of low-energy excited states [10, 11]. One of the main advantages of the instanton approach is that it can be readily extended to multidimensional systems using perturbative techniques (see [12] and references therein).

But before investigating multidimensional problems, we must study one-dimensional potentials and one-dimensional problems that cannot be accurately solved by the standard WKB method. These problems are the subject of this paper. The generalization of the instanton procedure to highly excited states is not straightforward at all, and required additional analysis. We consider only few relatively simple examples, but this analysis is useful for gaining insight into more complex systems for which even approximate theoretical results are not available.

In many interesting physical problems, high-accuracy calculations are out of reach of the standard WKB method, but as we see in what follows, the instanton approach offers a solution to the difficulties inherent to the WKB procedure. Since this fact was largely unnoticed in the previous studies, we found it worthwhile to present the investigation of several simple examples in a short and explicit form and to point out practical usability of the instanton approach. Apart from the aim to illustrate the efficiency of the instanton approach, our study is a prerequisite for an explanation and successful description of many relevant physical phenomena (for example, low-temperature quantum kinetics of phase transitions, see, e.g., [13]) where an active (reaction) path is effectively confined to one dimension.

All examples considered in this paper are related to the fundamental problems of chemical dynamics and molecular spectroscopy (see, e.g., [9] and references therein). Symmetric or slightly asymmetric double-well potentials are characteristic of molecules and Van der Waals complexes with more than one stable configurations [14–17]. The states of such systems close to the barrier top (theoretically described by the instanton approach in this paper) are most relevant for radiationless evolution of highly excited states. These states have a double (localized–delocalized) nature, which manifests itself in the wave functions that simultaneously contain both components, the localized component in one of the wells and the delocalized component between the two wells. The states close to the barrier top of decay potentials govern thermally activated over-barrier transition amplitudes. For low-energy states, the main reduction factor is the tunneling exponent, while the contribution of highly excited states is limited by the Boltzmann factor. Our instanton calculations demonstrate that there is no sharp boundary between quasistationary and delocalized states. Two of us (V. B. and E. K.) recently investigated [18] the eigenstates of a highly asymmetric double-well potential. We have shown that quantum irreversibility phenomena occur when the spacing between neighboring levels of the deeper well becomes smaller than the typical transition matrix element. Obviously, this criterion can also be applied to the states near the barrier top. We note that for low-energy states, the asymmetry leading to irreversible behavior must be very large, whereas for states near the barrier top, the condition of the ergodic behavior is not very severe, and it is sufficient for the

asymmetry of the potential to be comparable to the barrier height.

This paper is organized as follows. Section 2 contains the basic equations of the instanton method that are necessary for our investigation. As an illustration of the method, we consider a touchstone quantum mechanical problem — penetration of a particle through a parabolic potential barrier. The instanton solutions that are the asymptotic forms of the Weber equation are then exact. Section 3 is devoted to the investigation of highly excited states in a double-well potential. For concreteness and simplicity, we study the quartic anharmonic potential X^4. The instanton approach allows us to accurately reproduce not only the asymptotic behavior but also the crossover region from the single-well to the double-well quantization. In Sec. 4, a similar problem for the X^3 anharmonic potential is studied. Section 5 is devoted to the so-called resonance tunneling phenomena, which are not only interesting in their own right but also they play a relevant role in many semiconducting double-barrier structures. In Sec. 6, we discuss the results. In the Appendix, we compute the so-called connection matrices that provide a very efficient method of finding semiclassical solutions to the Schrödinger equation in potentials having several turning points. Knowing the connection matrices is also important and significant for developing a good analytical approximation. The readers not interested in the mathematical derivation can skip the Appendix and find all the results in the main body of the paper.

2. PENETRATION THROUGH THE PARABOLIC POTENTIAL BARRIER

2.1. Instanton approach

For convenience, we recall the main ideas of the instanton approach. The first step of the approach in [7] and [8] is the so-called Wick rotation of phase space corresponding to the transformation to imaginary time $t \to -it$. The potential and the kinetic energy change their signs after the transformation and the Lagrangian is replaced by the Hamiltonian in the classical equation of motion. By this Wick rotation, the standard oscillating WKB wave functions are transformed into exponentially decaying functions that vanish as $X \to \pm\infty$. Following [10, 11], we use a slightly different formulation of the instanton method, assuming exponentially decaying real-valued wave functions from the very beginning. Taking into account that the wave functions of bound states can be chosen as real quantities, we can therefore seek a solution to the Schrödinger equation in the form

$$\Psi = \exp\left(-\gamma\sigma(X)\right), \tag{2.1}$$

where γ is the semiclassical parameter that is assumed to be sufficiently large ($\gamma \equiv m\Omega_0 a_0^2/\hbar$, where m is the mass of a particle, a_0 is a characteristic length in the problem, e.g., the tunneling distance, and Ω_0 is a characteristic frequency, e.g., the oscillation frequency around the potential minimum; in what follows, we set $\hbar = 1$, measuring energies in the units of frequency) and σ can be called the action; this function must satisfy the first-order differential equation of the Ricatti type,

$$\gamma^2\left[-\frac{1}{2}\left(\frac{d\sigma}{dX}\right)^2 + V(X)\right] + \gamma\left[\frac{1}{2}\frac{d^2\sigma}{dX^2} - \epsilon\right] = 0, \tag{2.2}$$

where $V(X)$ is the potential and ϵ gives particle eigenstates (energies). Here and in what follows, we use dimensionless variables ($\epsilon = E/\Omega_0$ for the energy, $V = U/\gamma\Omega_0$ for the potential, and $X = x/a_0$ for the coordinate, where E and U are the corresponding dimensional values of the energy and potential). We believe that $\gamma \gg 1$, and $\sigma(X)$ can therefore be expanded in the asymptotic series

$$\sigma(X) = W(X) + \gamma^{-1}W_1(X) + \gamma^{-2}W_2(X) + \ldots \tag{2.3}$$

The first- and the second-order terms in γ^{-1} become identically zero if the time-independent Hamilton–Jacobi equation (HJE) and the so-called transport equation (TE) are satisfied,

$$\frac{1}{2}\left(\frac{dW}{dX}\right)^2 = V(X), \tag{2.4}$$

and

$$\frac{dW}{dX}\frac{dA}{dX} + \frac{1}{2}\frac{d^2W}{dX^2}A = \epsilon A, \tag{2.5}$$

where

$$A(X) \equiv \exp(-W_1(X)). \tag{2.6}$$

An essential advantage of the instanton method in comparison to the standard WKB is that in the former approach, the HJE is solved at $E = 0$, and the classically allowed regions therefore disappear. The price to be paid for this is the appearance of second-order turning points (in contrast to the WKB method, where all turning points are linear).

It is well known that the WKB wave functions are singular at the turning points, and therefore, different approximations represent the same wave function in different domains. The famous Stokes phenomenon [2] is related to the distribution of the turning points; Stokes and anti-Stokes lines emanate from each turning point. By definition, Stokes lines are the lines where the dominance of the dominant exponential semiclassical solution to the Schrödinger equation becomes strongest, and anti-Stokes lines are the lines on which the dominance and subdominance of the solutions interchange. Evidently, the WKB approximation does not work and must be refined near Stokes and anti-Stokes lines [2]. On the contrary, because classically accessible regions do not exist in the instanton formalism, the Stokes lines continuously pass through second-order turning points, and globally uniform real solutions to the Schrödinger equation can be constructed using the asymptotically smooth transformation of the instanton wave functions into the Weber functions. This global uniformity is the principal advantage of the instanton method.

A clearer idea of the instanton approach is obtained by the derivation of the well-known [1] quantization rules for the harmonic oscillator ($V(X) = X^2/2$). For a given energy ϵ, any solution of the Schrödinger equation can be represented as a linear combination of the solutions of the Weber equation [19]

$$\frac{d^2\Psi}{dz^2} + \left(\nu + \frac{1}{2} - \frac{z^2}{4}\right)\Psi(z) = 0, \tag{2.7}$$

where $z \equiv X\sqrt{\gamma}$ and $\nu = \epsilon - 1/2$. The basic solutions of (2.7) are the parabolic cylinder functions [19], and only the function $D_\nu(-z)$ vanishes as $z \to \infty$ for $\arg z = 0$. For $\arg z = \pi$, the asymptotic behavior of this function as $z \to \infty$ is given by [19]

$$D_\nu(-z) = \exp(i\pi\nu) z^\nu \exp\left(-\frac{z^2}{4}\right) - \\ - \frac{\sqrt{2}\pi}{\Gamma(-\nu)} z^{-\nu-1} \exp\left(\frac{z^2}{4}\right). \tag{2.8}$$

It can vanish as $z \to \infty$ only at the poles of $\Gamma(-\nu)$, and this vanishing condition gives the exact eigenvalues of the harmonic oscillator

$$\epsilon = n + \frac{1}{2}.$$

Moreover, because $D_\nu(-z)$ coincide with the known harmonic oscillator eigenfunctions for positive integer ν [1], the instanton approach to the harmonic oscillator is exact.

2.2. Tunneling through the harmonic barrier

As a less trivial illustration of the instanton approach efficiency, we apply the method to the problem of quantum mechanical tunneling through the parabolic potential

$$U(x) = U_0 - \frac{m\Omega_0^2}{2}x^2, \tag{2.9}$$

where m is the mass of the tunneling particle and Ω_0 is a characteristic frequency (the curvature of the potential). The potential involves an additional characteristic space scale a_0. Using Ω_0 and a_0 to set the corresponding scales, we can rewrite parabolic potential (2.9) in the dimensionless form

$$V(X) = V_0 - \frac{1}{2}X^2. \tag{2.10}$$

In these variables, the Schrödinger equation is given by

$$\frac{d^2\Psi}{dX^2} + (\gamma^2 X^2 - \alpha\gamma)\Psi(X) = 0, \tag{2.11}$$

where

$$\alpha = 2\frac{U_0 - E}{\Omega_0}, \tag{2.12}$$

and $\gamma \gg 1$ semiclassical parameter introduced above.

Schrödinger equation (2.11) can be transformed into the Weber equation [19] by a $\pi/4$-rotation in the complex plane,

$$X = \frac{1}{\sqrt{2}\gamma} z \exp\left(\frac{i\pi}{4}\right),$$

and the solution of (2.11) can therefore be represented as a linear combination of the parabolic cylinder functions D_ν [19],

$$\Psi_\nu(z) = c_1 D_\nu(z) + c_2 D_\nu(-z), \tag{2.13}$$

where $\nu = -1/2 - i\alpha/2$.

As $X \to \infty$, only the transmitted wave exists with the amplitude (the transmission coefficient) T,

$$\Psi \approx T \exp\frac{i\gamma X^2}{2}. \tag{2.14}$$

As $X \to -\infty$, both the incident wave ($\propto \exp(-i\gamma X^2/2)$) and the reflected wave proportional to $R\exp(i\gamma X^2/2)$ exist. By a standard quantum mechanical procedure [1], the transmission coefficient T and the reflection coefficient R can be found using the known asymptotic form of the parabolic cylinder

functions [19] at the fixed energy (i.e., at fixed α). This leads to the well known expression [1]

$$|T|^2 = \frac{1}{1+\exp(\pi\alpha)}. \tag{2.15}$$

We note that solutions (2.13) are the exact solutions to the Schrödinger equation in parabolic potential (2.10). We now apply the instanton approach described above to the same problem. The solutions of HJE (2.4) and TE (2.5), which are milestones of the method, can easily be found as

$$\begin{aligned} W &= \pm i\frac{X^2}{2}, \\ A &= A_0 X^{-1/2}\exp\left(\pm i\alpha\ln\frac{X}{2}\right), \end{aligned} \tag{2.16}$$

where the integration constant A_0 determines energy-dependent phases of the wave functions. Comparing (2.16) and (2.13), we can see that the instanton wave functions are the asymptotic forms of the parabolic cylinder functions, and therefore, because the transmission (T) and reflection (R) coefficients are determined only by the asymptotic behavior, the values of T and R found in the framework of the instanton approach coincide with the exact quantum mechanical ones at any value of the energy (of the parameter α). We recall that the instanton and the exact quantum mechanical solutions for the harmonic oscillator also coincide for any energy.

To finish this subsection, we mention for the skeptical reader that the WKB wave functions coincide with the exact solutions only at $\alpha \ll -1$. In the region where $|\alpha| \le 1$, i.e., where the characteristic size of the forbidden region becomes comparable to the particle wave length, specific interference phenomena between the transmitted and reflected waves occur, and phenomena of this kind cannot be reproduced in the standard WKB approach assuming that all turning points are independent.

As an illustration, in Fig. 1, we show the energy (α) dependence of the phase for the wave function reflected by the parabolic potential. The exact quantum mechanical and the instanton solutions (ϕ_0 in Fig. 1) are indistinguishable over a broad region of energies, while the WKB solution (ϕ_0^{WKB} in Fig. 1) deviates from both of them.

2.3. Connection matrices

Our analysis can be recast into a more elegant form by introducing the so-called connection matrices. In

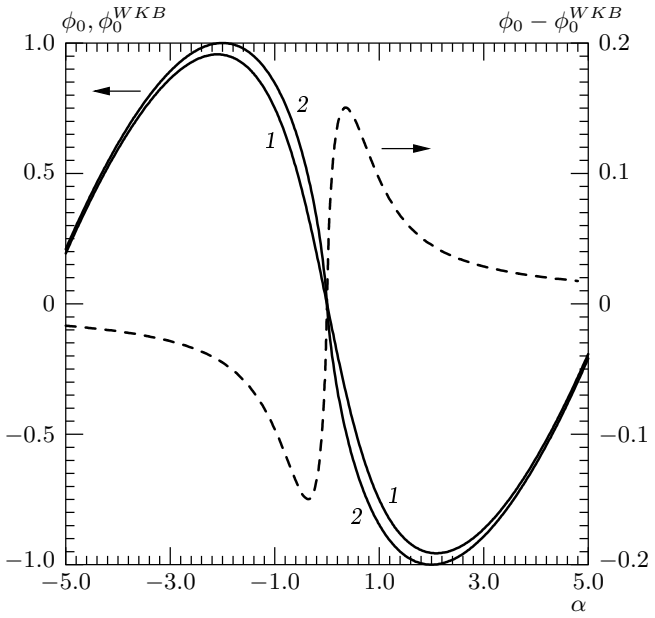

Fig. 1. The phase of the wave reflected from the parabolic barrier: *1* — the exact quantum and instanton solutions ϕ_0; *2* — the WKB solution ϕ_0^{WKB}; the dashed line is the difference $\phi_0 - \phi_0^{WKB}$

the instanton approach (as in any semiclassical treatment of the scattering or transition processes), we deal with only the asymptotic solutions and their connections on the complex coordinate plane. It is therefore important to know the connection matrices. These connection matrices provide a very efficient method of finding semiclassical solutions to the Schrödinger equation in potentials with several turning points. This is also a relevant starting point for developing a good analytical approximation.

It is convenient to formulate the general procedure for calculating the connection matrices for an arbitrary combinations of the first- and second-order turning points. The procedure can then be applied to any particular problem under investigation. Technically, this requires extending the procedure known for linear turning points [2]. All the necessary details of the generalization are given in the Appendix, and we here present only the main definitions and results. In the semiclassical limit $\gamma \gg 1$, the Stokes and anti-Stokes lines for the equation

$$\frac{d^2\Psi}{dz^2} + \gamma^2 q(z)\Psi(z) = 0 \tag{2.17}$$

are determined by the respective conditions

$$\operatorname{Re} W(z) = 0 \tag{2.18}$$

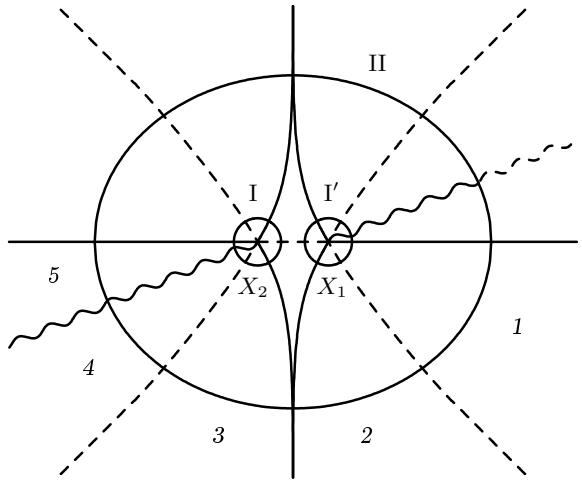

Fig. 2. The Stokes (solid) and anti-Stokes (dashed) lines for the two real-valued turning points $X_{1,2}$ with the surrounding contours I and I′. On contour II, the Stokes lines for the Airy equation asymptotically matches the lines for the Weber equation. The cut is depicted by the wavy line

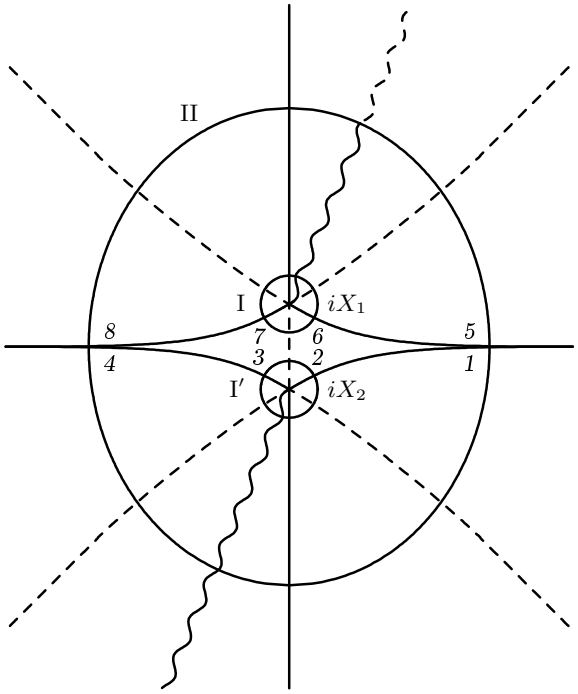

Fig. 3. The same as Fig. 2 for the case of two purely imaginary turning points $iX_{1,2}$

and

$$\operatorname{Im} W(z) = 0, \tag{2.19}$$

where

$$W(z) = \int_{z_0}^{z} \sqrt{q(z)}dz \tag{2.20}$$

and z_0 is the turning point under consideration.

For the harmonic potential, there are only linear turning points for real ($\alpha > 0$) and imaginary ($\alpha < 0$) energies. In the Appendix, we calculate all the connection matrices that we need. To fully analyze the problem for the entire range of parameters, we must therefore know only the distributions of turning points and the Stokes and anti-Stokes lines on the complex plane. At real turning points ($\alpha > 0$) where $X_{1,2} = \pm(\alpha/\gamma)^{1/2}$, there are four Stokes and four anti-Stokes lines and two cuts in the complex plane (see Fig. 2).

For $\alpha \gg 1$, the connection matrix can be easily calculated as the direct product of the connection matrices found in the Appendix ($\hat{M}^-$ in Eq. (A.4) and the Hermitian conjugate matrix $\hat{M}^+$) and the diagonal shift matrix

$$\begin{pmatrix} \exp(\pi\alpha/2) & 0 \\ 0 & \exp(-\pi\alpha/2) \end{pmatrix}. \tag{2.21}$$

This leads to the transmission coefficient $T \approx \approx \exp(-\pi\alpha/2)$, which coincides with (2.15) with the exponential accuracy in the limit $\alpha \gg 1$. To improve the accuracy at smaller values of α, we must calculate the connection matrices taking into account not only the contributions of the contours encompassing the turning points, but also the additional contribution to the action of the closed path (with a radius $\gg |X_{1,2}|$) encompassing both points X_1 and X_2 (see Fig. 2). The procedure changes the Stokes constant T_3 (on the dashed line separating regions *3* and *4* in Fig. 2), which becomes

$$|T_3| = [1 + \exp(-\pi\alpha)]^{1/2}.$$

This finally leads to the correct transmission coefficient

$$T = iT_3^{-1} \exp\left(-\frac{\pi\alpha}{2}\right),$$

which is identical to (2.15).

In the case where $\alpha < 0$, the entire picture (see Fig. 3) of the Stokes and of the anti-Stokes lines and turning points is rotated by the angle $\pi/2$ with respect to the picture in Fig. 2. If we bluntly take the point $X = 0$ as the low integration limit for the action W^* in Eq. (A.11), we obtain the transmission coefficient

$$T = 1 - \frac{1}{2}\exp(-\pi|\alpha|),$$

which can be reliable (with the accuracy $\exp(-2\pi|\alpha|)$) only for $|\alpha| \gg 1$. As in the case where $\alpha > 0$, the accuracy can be improved by taking into account the contribution of the path surrounding both imaginary turning points (this fact was noticed by Pokrovskii and Khalatnikov long ago [3]).

At the isolated linear imaginary turning point iX_1, the connection matrix is found from (A.4),

$$\tilde{M}_1^+ = \begin{pmatrix} 1 & i\exp(-\pi|\alpha|/2) \\ 0 & 1 \end{pmatrix}. \tag{2.22}$$

Similarly, the Hermitian conjugate matrix $\tilde{M}_1^-$ comes from the contribution of the closed path surrounding $-iX_1$. These contours provide only the amplitude of the dominant (exponentially increasing) wave. But the accuracy is insufficient for finding the amplitude of the corresponding subdominant solution (the exponentially decaying wave function), and we obtain the incorrect transmission coefficient $T = 1$. To improve the accuracy and to find T correctly, we must include the connection matrix for the isolated second-order turning point in the procedure (in this particular example, this turning point is the maximum of the potential). Using (A.9), we can explicitly find this matrix as

$$\tilde{M}_2 = \begin{pmatrix} [1+\exp(-\pi|\alpha|)]^{1/2} & i\exp(-\pi|\alpha|/2) \\ -i\exp(-\pi|\alpha|/2) & [1+\exp(-\pi|\alpha|)]^{1/2} \end{pmatrix}. \tag{2.23}$$

In principle, similar calculations can be performed in the adiabatic perturbation theory (which in fact employs the Planck constant smallness equivalent to $\gamma \gg 1$). We note that in [20], the contributions of the contours surrounding turning points (analogous to those presented above) were taken into account. It seems very plausible that following this way, it will be possible to combine the instanton approach and the adiabatic perturbation theory, but this issue is beyond the scope of this paper and will be discussed elsewhere.

3. HIGHLY EXCITED STATES IN THE DOUBLE-WELL POTENTIAL

Literally, the instanton approach described in the previous section is valid for states with characteristic energies that are small compared to the barrier height. But as we show in this section, the instanton method works sufficiently well for the energy states near the barrier top V_0. As an illustration, we consider the symmetric double-well potential (quartic anharmonic X^4 potential)

$$V_0 - V(X) = \frac{1}{2}X^2(1 - X^2). \tag{3.1}$$

The Schrödinger equation with potential (3.1) can be rewritten in dimensionless variables in the form

$$\frac{d^2\Psi}{dX^2} + [2\gamma^2(V_0 - V(X)) - \alpha\gamma]\Psi(X) = 0, \tag{3.2}$$

that is most convenient in applications of the instanton approach. The HJE and TE then become

$$\frac{1}{2}\left(\frac{dW}{dX}\right)^2 = V_0 - V(X), \tag{3.3}$$

and

$$\frac{dW}{dX}\frac{dA}{dX} + \frac{1}{2}\left(\frac{d^2W}{dX^2} + i\alpha\right)A = 0. \tag{3.4}$$

Formal solutions to the set of equations (3.3), (3.4) are the even and odd instanton wave functions

$$\Psi_I^{\pm} = A_{\pm}(X)\exp(i\gamma W_{\pm}(X)), \tag{3.5}$$

where the action $W_{\pm}$ (a solution of the HJE) is to be determined from

$$\frac{dW_{\pm}}{dX} = \pm\sqrt{2(V_0 - V(X))}, \tag{3.6}$$

and the amplitude (prefactor) is given by

$$A_{\pm} = \left|\frac{dW_{\pm}}{dX}\right|^{-1/2} \times \exp\left[-i\alpha\int\left(\frac{dW_{\pm}}{dX}\right)^{-1}dX\right]. \tag{3.7}$$

The quantization rules [1] are related to continuous matching of the solutions at the turning points (the second-order turning point $X = 0$ and the linear turning points $X = \pm 1$ for $\alpha > 0$ and $X = \pm i$ for $\alpha < 0$). A crucial advantage of instanton solutions (3.5) is that these functions have no singularities inside the barrier, because the corresponding exponents are pure imaginary in the classically accessible regions (unlike the WKB solutions). In addition, the general form of the instanton wave functions does not noticeably depend on whether $E < V_0$ or $E > V_0$. This advantage allows us to include the instanton wave functions into the basis of globally uniform functions diagonalizing the Hamiltonian even for highly excited states.

The above general procedure for searching instanton solutions to the Schrödinger equation with model potential (3.1) has a subtle point, which motivates giving the explicit searching procedure in some detail; new results follow from our investigation. The procedure includes several steps.

1. Near the second order turning point, exact solution (2.14) to the Schrödinger equation can be used with $c_1 = \pm c_2$ for the even and odd solutions respectively. For $|X| \gg 1$, it follows from (2.14) and from the known asymptotic forms of the parabolic cylinder functions [19] that

$$\Psi(X) = \frac{c_1}{\sqrt{X}} \times \times \left[\frac{\exp(if(X))}{\Gamma((1-i\alpha)/4)} + \frac{\exp(-if(X))}{\Gamma((1+i\alpha)/4)}\right], \quad (3.8)$$

where

$$c_1 = -\frac{2\pi}{\Gamma((3+i\alpha)/4)} \times \times \exp\left(-\frac{\pi\alpha}{8}\right) 2^{-i\alpha/4}(2\gamma)^{-1/4}, \quad (3.9)$$

and

$$f(X) = \frac{\gamma}{2}X^2 - \frac{\alpha}{2}\ln X - \frac{\alpha}{4}\ln\gamma - \frac{\pi}{8}. \quad (3.10)$$

To obtain the correct even and odd linear combinations conforming to (3.5), we set

$$c_\pm = c_1 \frac{\exp(\pm if_1)}{\Gamma((1 \pm i\alpha/\sqrt{2})/4)}, \quad (3.11)$$

where

$$f_1 = \frac{\alpha\ln\gamma}{4} + \frac{\pi}{8}.$$

2. Near the linear turning point $X = \pm 1$, the Schrödinger equation reduces to the Airy equation [19]

$$\frac{d^2\Psi}{dy^2} - y\Psi(y) = 0, \quad (3.12)$$

where

$$y = \gamma^{2/3}\left|X + 1 + \frac{\alpha}{\gamma}\right| \quad (3.13)$$

for $X < 0$. The solution that vanishes as $y \to \infty$ is given by [19]

$$\Psi(y) = |y|^{-1/4}\sin\left(\frac{2}{3}|y|^{3/2} + \frac{\pi}{4}\right). \quad (3.14)$$

Continuing this solution to the regions $(X \pm 1)\sqrt{2\gamma} \gg 1$ and sewing there with (3.8), we obtain

$$\frac{c_+}{c_-} = \exp\left(-i2\gamma W^* + i\frac{3\pi}{2}\right), \quad (3.15)$$

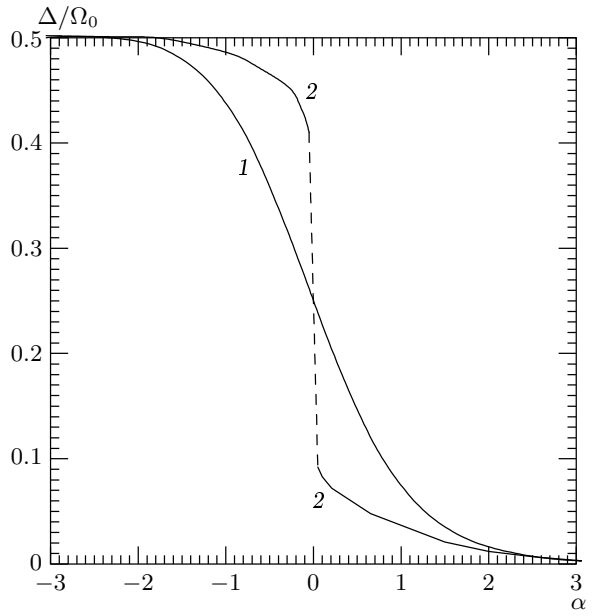

Fig. 4. The dimensionless tunneling splitting Δ/Ω_0 for the anharmonic X^4 potential near the barrier top: *1* — exact quantum and instanton calculations, *2* — the WKB result

where W^* is the energy-dependent action on the interval $[X = 0,\ X = 1]$.

3. Comparing (3.15) and (3.11), we find the quantization rules

$$\frac{\Gamma((1+i\alpha)/4)}{\Gamma((1-i\alpha)/4)} = \exp\left(-2i\gamma W^* - i\frac{3\pi}{2}\right) \quad (3.16)$$

for the even states and

$$\frac{\Gamma((3+i\alpha)/4)}{\Gamma((3-i\alpha)/4)} = \exp\left(-2i\gamma W^* - i\pi\right) \quad (3.17)$$

for the odd states.

4. From (3.16) and (3.17), we finally obtain the quantization rule that can be written in the single form for both the even and odd states as

$$2\gamma W^* + 2\phi(\alpha) \equiv \equiv \begin{pmatrix} \frac{5\pi}{4} + 2\pi n - \operatorname{arctg}\left(\operatorname{th}\left(\frac{\pi\alpha}{4}\right)\right) \\ \frac{3\pi}{4} + 2\pi n - 2\operatorname{arctg}\left(\operatorname{th}\left(\frac{\pi\alpha}{4}\right)\right) \end{pmatrix}. \quad (3.18)$$

Relation (3.18) is the sought quantization rule that now allows us to use the advantages of the instanton method. For highly excited states (i.e., for $\alpha \ll -1$), it follows from (3.18) that

$$2\gamma W^* + 2\phi(\alpha) = \pi\left(n + \frac{1}{2}\right),$$

where n is an integer. For low-energy states ($\alpha \gg 1$), Eq. (3.18) reproduces the known quantization rule

$$\gamma W_L^* = \pi\left(n + \frac{1}{2}\right) \pm \frac{1}{2}\exp\left(-\frac{\pi\alpha}{2}\right),$$

where W_L^* is the action in the classically admissible region between the linear turning point in the left well,

$$\gamma W_L^* = \gamma W^* + \phi(\alpha). \tag{3.19}$$

We note an essential advantage of instanton quantization rule (3.18) compared to the traditional WKB formalism, where the quantization rules are totally different [1] in the tunneling and over-barrier regions. The instanton approach gives a single quantization rule, Eq. (3.18), which is valid in both regions and in addition, quite accurately describes the crossover behavior near the barrier top, where periodic orbits localized at separate wells transform into a common figure-eight orbit enclosing both wells.

We illustrate the results of this section in Fig. 4, where we plot the universal dependence of the eigenvalues in symmetric double-well potential (3.1) on α. For comparison, we show in the same figure the eigenvalues found by the conventional WKB procedure and by the exact quantum mechanical computation. It is clear from the figure that the WKB method errors are maximal in the region of small $|\alpha|$, because the oscillation period logarithmically diverges in this region (the particle spends infinitely long time near the second-order turning point). On the contrary, the errors of the instanton approach are minimal near the barrier top (small $|\alpha|$).

As mentioned at the beginning of this section, the instanton approach is also very accurate near the potential minimum. Generally speaking, the instanton solutions are always correct when the deviation from the corresponding extremum is of the order of characteristic zero-point amplitudes. Mathematically, the accuracy of the instanton approach is based on the transformation of the semiclassical solutions into the harmonic oscillator eigenfunctions (which also ensures the correct normalization of the instanton wave functions). It is therefore natural to expect that the instanton method is very accurate near the barrier top and near the potential minimum. On the contrary, in the intermediate region, where the anharmonic shape of the potential is relevant, we should expect poor accuracy of the instanton method. Fortunately, it turns out that the mathematical nature of the problem is on our side, and the instanton approach has a reasonable accuracy (of the order of the accuracy of the WKB method) even in this region. The fact is that the instanton wave functions are exact not only in zero but also in the first order with respect to anharmonic corrections to the potential approximation. This can be shown using the anharmonic perturbative procedure that was proposed by Avilov and Iordanskii for the WKB functions [21] and was generalized for the instanton wave functions in [22].

For practical computations, it is also relevant that the instanton wave functions (unlike the WKB ones) are continuous near their «own» minimum. Numerical estimate shows that in the intermediate energy region, the instanton wave functions reproduce exact quantum results with the accuracy about 5–10 %.

To finish the section, we present the connection matrices needed to find semiclassical solutions to the Schrödinger equation in the double-well potential. Similarly to the results in Sec. 2, the connection matrix for the instanton solutions is the product of connection matrices (A.4) for the linear turning points and the connection matrix for the second-order turning point, which is the maximum of the double-well potential in the case under consideration. Using (A.9), we can find this latter connection matrix as

$$\begin{pmatrix} 2\left[\exp\left(\frac{\pi\alpha}{2}\right) + (1+\exp(\pi\alpha))^{1/2}\cos(2\gamma W^*)\right] & -(1+\exp(\pi\alpha))^{1/2}\sin(2\gamma W^*) \\ (1+\exp(\pi\alpha))^{1/2}\sin(2\gamma W^*) & \frac{1}{2}\left[-\exp\left(\frac{\pi\alpha}{2}\right) + (1+\exp(\pi\alpha))^{1/2}\cos(2\gamma W^*)\right] \end{pmatrix}. \tag{3.20}$$

It is worth noting that the reflected wave acquires a nontrivial phase factor near the barrier top. This phenomenon is related to the interference of the incident, reflected, and transmitted waves, and the phase therefore has some geometrical meaning, similarly to the famous Berry phase [23]. The geometrical origin of the phase manifests itself more clearly if we recall that the semiclassical phase factor is determined by the probability density flow through the barrier,

$$J = i\Psi^*\frac{d\Psi}{dX}.$$

We can consider this phase factor from a slightly different standpoint, because tunneling results in a phase shift related to the change of the eigenvalues. Quantization rules (3.18) and (3.19) can be rewritten as

$$\epsilon_n = n + \frac{1}{2} + \chi_n,$$

which is the definition of the eigenvalues ϵ_n and where n is integer labeling the eigenvalues and χ_n is determined by the exponentially small phase shift due to the existence of the barrier between the two wells. The phase shift χ_n has the same functional form (and physical meaning) as the geometrical phase factor (appearing because of the interference phenomena) acquired by a quantum mechanical wave function upon a cyclic evolution [23–25].

4. THE DECAY POTENTIAL

In this section, we study highly excited states in a decay potential, which we choose as the anharmonic X^3 potential for definiteness,

$$V(X) = \frac{1}{2}X^2(1 - X). \tag{4.1}$$

As a first (but compulsory) step, we investigate the low-lying tunneling states.

4.1. Tunneling decay of metastable states

We start from this simple case to pick low-hanging fruits first, i.e., to describe the states under the conditions

$$V_0 \gg \epsilon_n \gg V(X \to \infty), \tag{4.2}$$

which imply that a local minimum is separated from the continuum spectrum by a high energetical barrier, and the quasistationary states ϵ_n are therefore characterized by «good» quantum numbers n. We note that a generic decay potential shown in Fig. 5 is determined by the positions of the barrier top X_0 and the three turning points $-X_1$, $X = 0$, and $+X_2$; near these points, we have

$$V(X) = \begin{cases} V_0 - \left(\dfrac{dV}{dX}\right)_{X=-X_1}(X+X_1), & |X+X_1| \to 0, \\ \dfrac{1}{2}X^2, & |X| \to 0, \\ V_0 - \dfrac{1}{2}(X - X_0)^2, & |X - X_0| \to 0, \\ -\left(\dfrac{dV}{dX}\right)_{X=X_2}(X-X_2), & |X-X_2| \to 0. \end{cases} \tag{4.3}$$

Potential (4.1) is a particular example of the generic decay potential in Eq. (4.3) (with $X_1 = 1/3$, $X_0 = 2/3$, $X_2 = 1$, and $V_0 = 2/27$); we use it only as an explicit illustration, and in order to be specific, while all the results given below are equally valid for the generic potential. As a note of caution, we also remark that in the instanton approach to this problem, we must always deal with only two turning points. For low-energy states, the points are X_2 and the potential minimum $X = 0$, and for high-energy states, the points are $-X_1$ and the potential maximum X_0.

In accordance with (4.1), there are no turning points at $X > X_2$; at $X \gg X_2$, the potential can be considered as a constant, and therefore the wave functions must therefore asymptotically coincide with plane waves for $X \gg X_2$. Furthermore, near the linear turning point $X = 1$, the Schrödinger equation with the X^3 anharmonic potential (4.1) is reduced to Airy equation (3.12), whose solutions are linear combinations of the Bessel functions with the indices $\pm 1/3$ at real (for $X < 1$) and imaginary (for $X > 1$) values of the arguments,

$$\Psi(u) = \sqrt{u} \times \left[B_+ I_{1/3}\left(\frac{2u^{3/2}}{3}\right) + B_- I_{-1/3}\left(\frac{2u^{3/2}}{3}\right)\right], \tag{4.4}$$

and

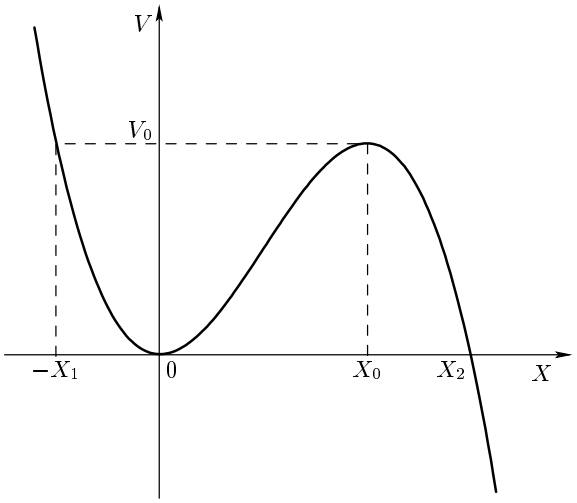

Fig. 5. The X^3 anharmonic decay potential

$$\Psi(\zeta) = \sqrt{\zeta} \times$$
$$\times \left[-B_+ J_{1/3}\left(\frac{2\zeta^{3/2}}{3}\right) + B_- J_{-1/3}\left(\frac{2\zeta^{3/2}}{3}\right)\right], \quad (4.5)$$

where

$$u = (2\gamma)^{2/3}\left[1 - X - \frac{\nu + 1/2}{\gamma}\right] \quad (4.6)$$

for $X < 1$ and

$$\zeta = (2\gamma)^{2/3}\left[X - 1 + \frac{\nu + 1/2}{\gamma}\right], \quad (4.7)$$

for $X > 1$ (we recall that $\nu = \epsilon_n - 1/2$ here).

The coefficients $B_\pm$ must be chosen such that Eq. (4.5) gives plane waves for $\zeta \gg 1$; using the known asymptotic forms of the Bessel functions [19], we thus obtain

$$B_+ = B_- \exp\left(-i\frac{\pi}{3}\right).$$

In the classically forbidden region $u \gg 1$, the instanton solutions of HJE (2.4) and TE (2.5) that continuously match the quantum mechanical solutions of the Schrödinger equation near the turning points are given by

$$\Psi_\pm = A_\pm \exp(\pm\gamma W), \quad (4.8)$$

where

$$A_\pm = X^{-1/2}(1-X)^{-1/4}\left(\frac{1-\sqrt{1-X}}{1+\sqrt{1-X}}\right)^{n\epsilon_n} \quad (4.9)$$

and

$$W = \frac{8}{15} - \frac{4}{3}(1-X)^{3/2} + \frac{4}{5}(1-X)^{5/2}. \quad (4.10)$$

The sought wave functions of the quasistationary states are linear combinations of instanton solutions (4.8), with the coefficients in the linear combinations determined from the condition of asymptotically matching the parabolic cylinder functions in Eq. (2.13) and the Airy functions. This leads to the following equation for complex eigenvalues ν:

$$-\frac{\sqrt{2\pi}}{\Gamma(-\nu)}\exp\left(\frac{16}{15}\gamma\right) = i\gamma^{\nu+(1/2)}2^{6\nu+3}. \quad (4.11)$$

Because the function $\Gamma(z)$ has a simple pole at $z = -n$, we can easily find the leading contribution to the decay rate Γ_n of the quasistationary state ϵ_n,

$$\frac{\Gamma_n}{\Omega_0} = \sqrt{\frac{2}{\pi}}\frac{\gamma^{\nu+1/2}2^{6\nu+3}}{n!}\exp\left(-\frac{16}{15}\gamma\right). \quad (4.12)$$

We note that for the ground state, with $n = 0$, Eq. (4.12) coincides with the result found by Caldeira and Legget [26]. On the other hand, the decay rate is related to the current flow [1] as $X \to +\infty$, providing the constant amplitude of the outgoing wave,

$$\frac{\Gamma_n}{\Omega_0} = \left(2i\sqrt{\gamma}\int|\Psi|^2 dX\right)^{-1} \times$$
$$\times \left(-\Psi^*\frac{d\Psi}{dX} + \Psi\frac{d\Psi^*}{dX}\right). \quad (4.13)$$

Inserting the explicit forms of the wave functions in Eqs. (4.5), (4.6), and (4.7) in (4.13), we obtain

$$\frac{\Gamma_n}{\Omega_0} = \frac{9}{8}\frac{\gamma^{1/6}}{2^{1/3}}|B_+|^2. \quad (4.14)$$

In accordance with (4.14), the decay rate depends only on the normalization of the instanton wave function and on the amplitude of the outgoing wave. Both characteristics are determined essentially by the behavior of the instanton wave function in the vicinity of the turning points only. We note, however, that in this approximation, the instanton computation of decay rate (4.13) or (4.14) is satisfactory only for the ground state, because corrections of the order γ^{-1} rapidly increase with the quantum number n. The method can be improved by taking the X^3 anharmonic contribution to the potential into account as a perturbation,

$$\frac{\Gamma_n}{\Omega_0} = \sqrt{\frac{2}{\pi}}\frac{\gamma^{\nu+1/2}2^{6\nu+3}}{n!}\exp\left(-\frac{16}{15}\gamma\right) \times$$
$$\times \left[1 - \frac{1}{576\gamma}(164n^3 + 246n^2 + 1216n + 567)\right]. \quad (4.15)$$

The decay rate calculated in accordance with (4.15) is of the same accuracy level as the WKB and the exact quantum mechanical computations for $\gamma \geq 5$. Outside the regime of interest, the instanton theory loses all pretence of predictability.

4.2. Highly excited states for the anharmonic X^3 potential

In Sec. 4.1, we calculated the decay rate of low-energy metastable states. In this case (where the states ϵ_n can be characterized by the good quantum number n), the period of oscillations in the well is smaller than the inverse decay rate ($\epsilon_n \gg \Gamma_n/\Omega_0$) and Γ_n is determined by the probability current density flowing from the well into the classically admissible region ($X > X_0$ for a given energy ϵ_n, see Fig. 5) under the condition of the vanishing back-flow from this region to the barrier. Evidently, the method does not work for highly excited states with $\Gamma_n \geq \epsilon_n \Omega_0$. In this Section, we go one step further with respect to Subsec. 4.1 in extending the instanton approach to the decay of highly excited states.

First, it is worth noting that the wave functions must vanish as $X \to -\infty$, and moreover, can always be chosen as real-valued quantities as $X \to +\infty$. From these two conditions, we can find the relations between the instanton wave functions in the regions $X < -X_1$ and $X > X_0$ (see the notation in Fig. 5), and consequently, calculate the phase $\delta(\alpha)$ (counted from the barrier top) of the standing wave in the region $X > X_0$. It is given by

$$\exp(i2\delta) = -i\exp(-i2\gamma W^*) \times \times \left\{1 + \frac{\sqrt{2\pi}\exp(-\pi\alpha/4)\exp(i2\gamma W^*)}{\Gamma(1-i\alpha/2)}\right\} \times \times \left\{1 + \frac{\sqrt{2\pi}\exp(-\pi\alpha/4)\exp(-i2\gamma W^*)}{\Gamma(1+i\alpha/2)}\right\}^{-1}. \quad (4.16)$$

According to the standard quantum mechanics [1], phase (4.16) determines the scattering amplitude. We can therefore find the scattering amplitude deep in the classically forbidden region from (4.16), and hence, compute the eigenvalues in this region. For the calculation, we must know the terms of the order $\exp(-\pi|\alpha|)$ in the expansion of the Γ functions (these terms are beyond the standard Stirling formula) [19],

$$\Gamma\left(\frac{1 \pm i\alpha}{2}\right) \approx \sqrt{2\pi}\exp\left(-\frac{\pi\alpha}{4} \pm i\phi\right) \times \times \left[1 - \frac{1}{2}\exp(-\pi|\alpha|)\right], \quad (4.17)$$

where

$$\phi(\alpha) \equiv \frac{\alpha}{2}\left[\ln\frac{|\alpha|}{2} - 1\right]. \quad (4.18)$$

Finally, taking Eqs. (4.17) and (4.18) into account we find the poles of the scattering amplitude from (4.16) (with the required exponential accuracy) as

$$2\gamma W_L^* = 2\gamma W^* + \phi(\alpha) = \pi(2n+1) - - i\left[\frac{\pi}{4}(|\alpha| - \alpha) + \frac{1}{2}\exp(-\pi|\alpha|)\right]. \quad (4.19)$$

Explicitly solving (4.19), we find the complex eigenvalues, and in particular, the decay rate for highly excited states in the anharmonic decay potential.

In the same way as for low-energy tunneling states, the real part of the eigenvalues ϵ_n for highly excited states (i.e., for $|\alpha| \gg 1$) is determined by the action along closed trajectories in the well, whereas the imaginary part (i.e., the decay rate Γ_n) is related to the probability current density flow from the well to the barrier.

Using the instanton approach procedure described in Secs. 2 and 3 (see [10, 11] for the details), we can find not only the eigenvalues but also the eigenstates. The real-valued instanton wave functions are determined by the action $W(X_1, X)$, which is counted from the linear turning point X_1,

$$\Psi(X) = A(\alpha)|X - X_1|^{-1/4} \times \times \sin\left(\gamma W(X_1, X) + \frac{\pi}{4}\right), \quad (4.20)$$

where the amplitude $A(\alpha)$ of the wave function acquires maximum values at the poles of (4.16) with the widths proportional to Γ_n. We plot the functions $|A(\alpha)|^2$ in Fig. 6.

5. RESONANCE TUNNELING

The phenomenon of the electron resonance tunneling is familiar [27] and was observed (see, e.g., [28] and also [29] for more recent references) in semiconducting heterostructures possessing the so-called double-barrier potentials (see Fig. 7). This phenomenon manifests itself as peaks in the tunneling current at voltages near the quasistationary states of the potential well. The physical mechanism of the resonance tunneling can be understood as a constructive interference between the wave reflected from the left barrier and the wave outgoing to the left of the well.

In the instanton method, the total transmission coefficient T is determined by the second-order turning

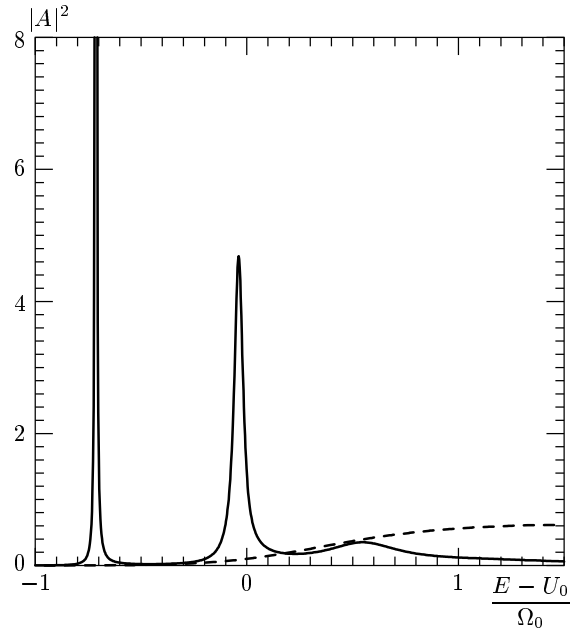

Fig. 6. The amplitude of the wave function localized in the potential shown in Fig. 5 (the dashed line is a nonresonant part of the amplitude and $\gamma = 101$)

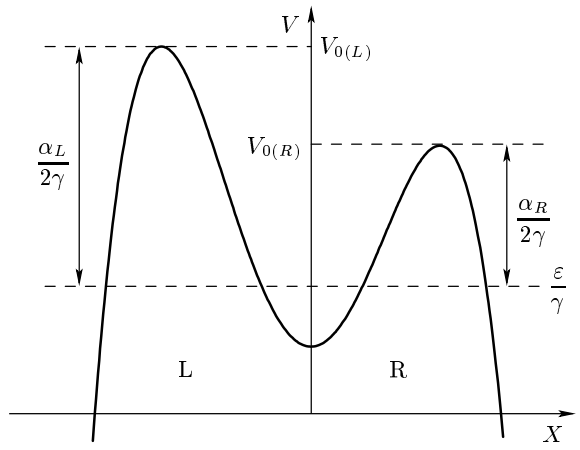

Fig. 7. The model two-barrier potential structure for the resonance tunneling

points of the double-barrier potential (i.e., the maxima of the potential); in accordance with the procedure described in the Sec. 2, T is given by

$$|T|^2 = \pi^2 \Gamma_L \Gamma_R \left\{ \left[1 - \sqrt{(1+\pi\Gamma_L)(1+\pi\Gamma_R)} \right]^2 + \right.$$
$$\left. + 4\sqrt{(1+\pi\Gamma_L)(1+\pi\Gamma_R)}\cos^2(\gamma W_R^*) \right\}^{-1}, \quad (5.1)$$

where we use the notation

$$\Gamma_{L,R} = \frac{1}{\pi}\exp(-\pi\alpha_{L,R}) \quad (5.2)$$

and similarly to (2.12),

$$\alpha_{L,R} = 2\frac{U_{0(L,R)} - E}{\Omega_{0(L,R)}}. \quad (5.3)$$

Similarly to (3.19), the action in the classically admissible region, is given by

$$\gamma W_R^* = \gamma W^* - \phi(\alpha_L) - \phi(\alpha_R). \quad (5.4)$$

In the resonance region, where

$$\gamma W_R^* = \pi\left(n + \frac{1}{2}\right)$$

in accordance with the stationary quantization rule, the transmission coefficient in (5.1) is given by

$$|T|^2 = \frac{4\Gamma_L\Gamma_R}{(\Gamma_L + \Gamma_R)^2}. \quad (5.5)$$

Far from the resonance, it is given by

$$|T|^2 = \frac{\pi^2\Gamma_L\Gamma_R}{4\cos^2(\gamma W_R^*)}. \quad (5.6)$$

We thus found the resonance amplification of the transmission. For the symmetric case at the resonance,

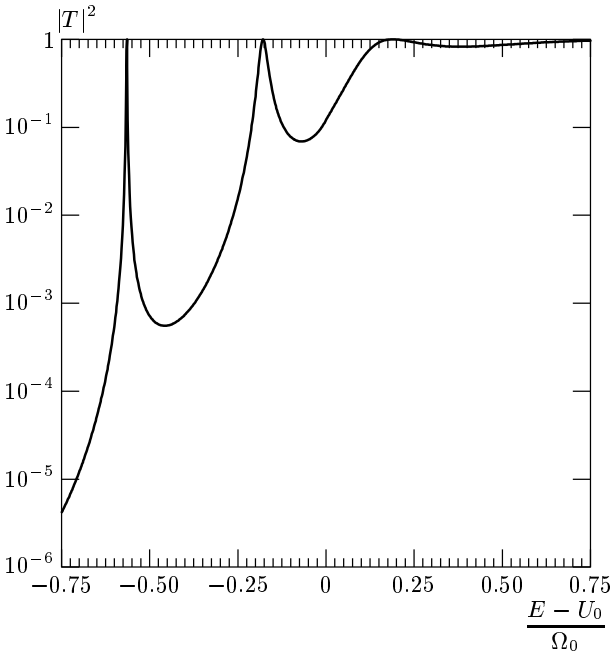

Fig. 8. The transmission coefficient for the potential shown in Fig. 7 ($\gamma = 54$)

$T = 1$, and the interference completely suppresses the reflection. In the opposite case of strongly asymmetric barriers, T in (5.1) is almost coincident with the transmission coefficient for the highest barrier, and the influence of the lower barrier is suppressed by the interference. In Fig. 8, we show the energy dependence of T for the symmetric structure of the barriers. The resonances become broader as the energy approaches the potential barriers top, and disappear at higher energies (above the top). It is worthwhile to stress that the instanton solution of the resonance tunneling problem allows us to study the phenomenon in a very broad energy region, including the states near the barriers tops.

We finally present the connection matrices for the instanton solutions found above. The corresponding matrix can be found as the product of two connection matrices connecting instanton solutions near the second order turning points (see (A.9) and (3.20)) and diagonal shift matrix (A.6),

$$\begin{pmatrix} 2\pi\exp\left(\pi\dfrac{\alpha_L+\alpha_R}{4}\right)\exp(i\gamma W^*)\left[\Gamma\left(\dfrac{1+i\alpha_L}{2}\right)\Gamma\left(\dfrac{1+i\alpha_R}{2}\right)\right]^{-1}+\exp\left(\pi\dfrac{\alpha_L+\alpha_R}{2}\right)\exp(-i\gamma W^*) \\ -i\sqrt{2\pi}\exp\left(3\pi\dfrac{\alpha_R+\alpha_L}{8}\right)\left[\exp(i\gamma W^*)\Gamma^{-1}\left(\dfrac{1+i\alpha_R}{2}\right)+\exp(-i\gamma W^*)\Gamma^{-1}\left(\dfrac{1-i\alpha_L}{2}\right)\right] \end{pmatrix}$$

$$\begin{pmatrix} i\sqrt{2\pi}\exp\left(3\pi\dfrac{\alpha_R+\alpha_L}{8}\right)\left[\exp(i\gamma W^*)\Gamma^{-1}\left(\dfrac{1+i\alpha_L}{2}\right)+\exp(-i\gamma W^*)\Gamma^{-1}\left(\dfrac{1-i\alpha_R}{2}\right)\right] \\ 2\pi\exp\left(\pi\dfrac{\alpha_L+\alpha_R}{4}\right)\exp(-i\gamma W^*)\left[\Gamma\left(\dfrac{1+i\alpha_L}{2}\right)\Gamma\left(\dfrac{1+i\alpha_R}{2}\right)\right]^{-1}+\exp\left(\pi\dfrac{\alpha_L+\alpha_R}{2}\right)\exp(i\gamma W^*) \end{pmatrix}. \quad (5.7)$$

Here, W^* denotes the action between the turning points (in this case, between the second-order turning points).

6. CONCLUSIONS

This paper could be considered as a formal one, in the sense that we asked theoretical questions that most of solid-state or chemical physics experimentalists would not think to ask. But answering these very basic questions can be illuminating.

We first summarize the results of the paper. Within the framework of the instanton approach, we derived accurate analytical solutions for a number of one-dimensional semiclassical problems and checked the results numerically. As an illustration of the method, we considered a simple quantum mechanical problem, penetration of a particle through the parabolic potential barrier. In this case, the instanton solutions (which are asymptotic solutions of the Weber equation) are exact. We also considered the description of highly excited states in a double-well potential. For definiteness and simplicity, we studied the quartic anharmonic X^4 potential. The instanton approach enables us to accurately reproduce not only the asymptotic behavior but also the crossover region from the single-well to the double-well quantization (in contrast to the standard WKB approach, which fails to describe the crossover behavior). A similar problem for the X^3 anharmonic potential was also studied, and the instanton method has allowed us to study the resonance broadening and collapse phenomena. In addition, we investigated the so-called resonance tunneling phenomena, not only interesting in their own right but also playing a relevant role in many semiconducting double-barrier structures. We also computed the connection matrices that provide a very efficient method of finding semiclassical solutions to the Schrödinger equation in potentials with several turning points (they are also useful in developing a good analytical approximation).

All the examples selected to illustrate the efficiency of the instanton approach belong to the fundamental problems in chemical dynamics and molecular spectroscopy (see, e.g., [9] and references therein). Symmetric or slightly asymmetric double-well potentials are characteristic of molecules and Van der Waals complexes with more than one stable configurations [14–17]. The states of such systems that are close to the barrier top (theoretically described by the instanton approach in our paper) are not easy to investigate experimentally, because optical transitions between these states and the localized ones are typically inactive. But

pecisely these states are most relevant for radiationless evolution of highly excited states. In a certain sense, these states have a double (localized–delocalized) nature that manifests itself in the form of wave functions that simultaneously contain both components, the one localized in one of the wells and the other delocalized between the two wells. Consequently, any initially prepared localized state evolves via formation and decay of these states. Our calculations are intended to pave the way to the investigation of this class of problems using the wave functions computed within the instanton approach.

The states that are close to the barrier top of decay potentials govern thermally activated over-barrier transition amplitudes. For low-energy states, the main reduction factor is the tunneling exponent, while the contribution of highly excited states is limited by the Boltzmann factor. The energy width of the region dominating in the total transition rate is traditionally postulated in the transition rate theory [30] to be of the order of the temperature T. But our results in Sec. 3 predict another estimate. Instanton calculations demonstrate that the intermediate region between the quasistationary ($\Gamma \ll \Omega$) and the delocalized states could be much larger than T, namely of the order Ω. This implies that no sharp boundary exists between the quasistationary and the delocalized states and all of the states within the interval $V^* - \Omega$, $V^* + T$ equally contribute to the total rate constant for the penetration through the barrier.

One more point should be emphasised. It was recently shown in [18] that quantum irreversibility phenomena occur when the spacing between neighboring levels of the deeper well becomes smaller than the typical transition matrix element. Obviously, this criterion can also be applied to the states near the barrier top. We note that for low-energy states, the asymmetry providing the irreversible behavior must be very large, whereas for states near the barrier top, the condition of the ergodic behavior is not very severe, it suffices that the asymmetry of the potential is comparable to the barrier height.

The method and the results can also be applied to various systems in physics, chemistry, and biology exhibiting double-level behavior and resonance tunneling. Literally speaking, we dealt with the microscopic Hamiltonians in this paper. But because of rapid development of electronics and cryogenic technologies, it has become possible to apply the same Hamiltonians to study cases where the corresponding variables are macroscopic (e.g., the magnetic flux through a SQUID ring, or charge or spin density wave phase in certain one-dimensional solids). In this paper, we studied the example of a tunneling processes in which the system penetrates into a classically forbidden region (a potential barrier). It is an intrinsically quantum effect with no classical counterpart, but it can nevertheless occur for macroscopic systems, and the tunneling of a macroscopic variable of the macroscopic system (e.g., spin or charge tunneling in atomic condensates trapped in a double-well potential [31]) can also be investigated by our method.

With this background in mind, our results are also intended to clarify different subtle aspects of tunneling phenomena. An example was given at the end of Sec. 3, where we found the geometrical phase acquired by a particle tunneling through a potential barrier. This phase can be tuned by the particle energy and by the barrier shape, and specific interference phenomena might occur. The observation of oscillations related to this geometrical phase in real systems has proved challenging. Evidently, because the forms of the model potentials that we used are rather special (and in addition, only one-dimensional), we cannot discuss the behavior for general cases with full confidence. Nevertheless, we believe that the instanton approach employed in this work should also be useful in deriving valuable results for the general and multidimensional potentials.

It is essential that in the instanton method discussed in this paper, a mere observating of several classical trajectories suffices to develop a qualitative insight for the quantum behavior. Although the semiclassical instanton approach is reliable in this context (as we illustrated in a number of particular examples), it is much more than a qualitative picture. As an approximation, the instanton method can be surprisingly precise. We also note that the results presented here are not only interested in their own right (at least in our opinion) but may also be directly tested experimentally, because there are many systems where the model investigated in the paper is a reasonable model of the reality.

The theory presented in our paper could be extended in several directions. One very interesting question is how our quantum mechanical instanton formulas (e.g., Eqs. (4.12)–(4.14) for the tunneling rate in the anharmonic X^3 decay potential) are modified by interactions with the surrounding media (see, e.g., [32], where the WKB approach was used to study the time evolution of quantum tunneling in a thermally fluctuating medium). Theoretical modeling of this case is hampered by the absence of detailed knowledge of the medium and of the interaction with it. A more specific

study might become appropriate once suitable experimental results become available. A simple criterion for the strength of the interaction with the environment (in other words, for the effective temperature) for the crossover from the thermally activated classical to quantum mechanical decay can easily be found by equating the corresponding Arrhenius factor and the characteristic frequency «oscillations» inside the barrier Ω_* (see (A.10)).

All of the potentials investigated in this paper can be considered in a number of realistic cases as effectively resulting from avoiding the adiabatic level crossing in the situation where the adiabatic splitting is so large that any influence of the upper adiabatic states on the lower states can be neglected. Certainly, in the general case of an arbitrary coupling strength, this interaction of higher and lower adiabatic states must be taken into account, and the tunneling matrix elements must be accompanied by the corresponding Franck–Condon factors arising because of the violation of the Born–Oppenheimer approximation. We defer these problems to the future, although there is no doubt that the instanton approach is also useful in problems of this kind.

The research described in this publication was made possible in part by the RFBR (grants 00-03-32938 and 00-02-11785).

APPENDIX

Following [2], we introduce short notations for the standard basic WKB solutions,

$$(\circ, z) \equiv (q(z))^{-1/4} \exp(i\gamma W(z)), \qquad (A.1)$$

and

$$(z, \circ) \equiv (q(z))^{-1/4} \exp(-i\gamma W(z)). \qquad (A.2)$$

The position of the turning point is denoted by $\circ$ and is inessential if we seek solutions in the region $|z| \gg 1$. In accordance with definitions (2.18), and (2.19), we must add the dominant solution times a certain constant (the Stokes constant) to the subdominant (decaying) solution on the Stokes lines; the dominant and the subdominant solutions are exchanged on the anti-Stokes lines. To find the Stokes constant, we must match both solutions by encompassing the turning point and taking the cut on the complex z plane into account (see Fig. 9).

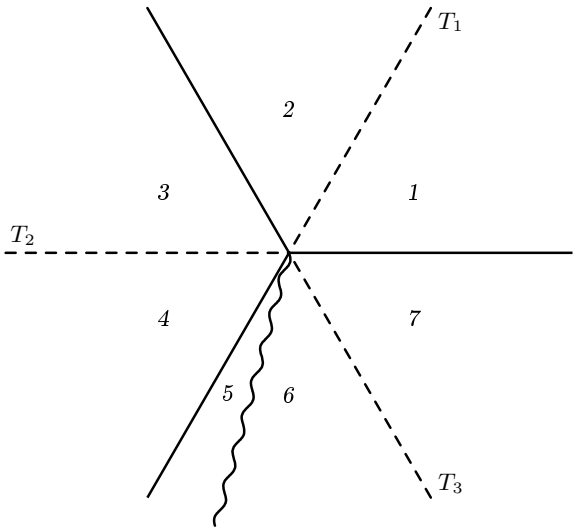

Fig. 9. The Stokes (solid) and anti-Stokes (dashed) lines in the vicinity of the linear turning point $V(X) = -X$. The cut is depicted by the wavy line, and the Stokes constant are T_1, T_2, and T_3

We first consider the linear turning point

$$q(z) = -z, \qquad (A.3)$$

with the classically admissible region corresponding to $X > 0$. In this case, we have three Stokes lines, three anti-Stokes lines, one cut, and therefore, seven different regions on the complex z-plane where functions (A.1) and (A.2) must be matched; as a result, three Stokes constant must be determined. After not very sophisticated but rather tedious algebraic calculations, we find all the three Stokes constants

$$T_1 = T_2 = T_3 = i,$$

and the connection matrix

$$\hat{M}^- = \exp\left(-i\frac{\pi}{4}\right) \times \times \begin{pmatrix} \exp(i\pi/4 & (1/2)\exp(-i\pi/4) \\ \exp(-i\pi/4) & (1/2)\exp(i\pi/4) \end{pmatrix} \qquad (A.4)$$

relating the coefficients of the linear combinations of basic solutions (A.1) and (A.2) in the classically forbidden region (A_1, A_2) and in the classically admissible region (A_2, B_2) as

$$\begin{pmatrix} A_2 \\ B_2 \end{pmatrix} = \hat{M}^- \begin{pmatrix} A_1 \\ B_1 \end{pmatrix}. \qquad (A.5)$$

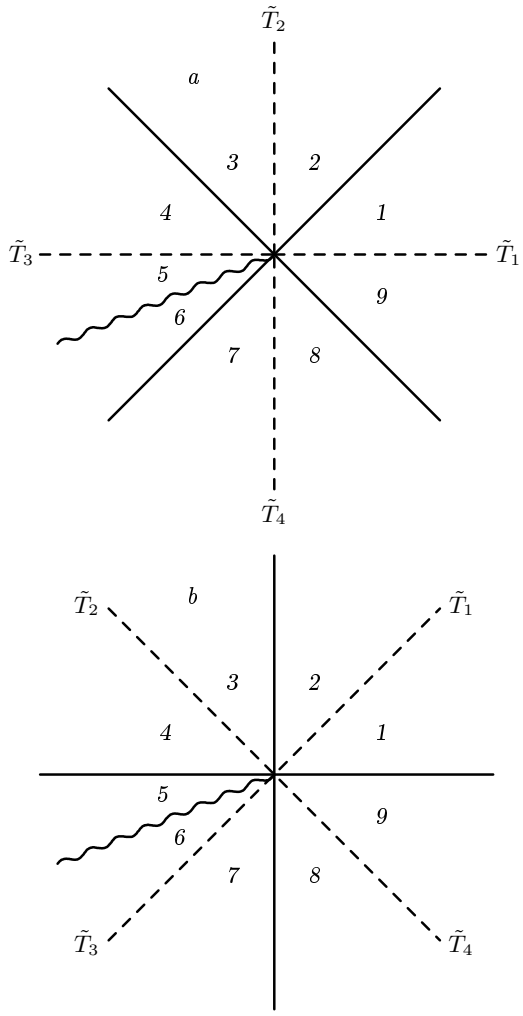

Fig. 10. The Stokes and anti-Stokes lines in the vicinity of the second-order turning points (with the same notation as in Fig. 9); a — $V(X) = (1/2)X^2$, b — $V(X) = -(1/2)X^2$

For the other linear turning point $q(z) = +z$, the connection matrix $\hat{M}^+$ is Hermitian conjugate to $\hat{M}^-$. The variation of the coefficients in the region between the two independent linear turning points z_1 and z_2 is determined by the diagonal matrix

$$\hat{L} = \begin{pmatrix} \exp(-i\gamma W^*) & 0 \\ 0 & \exp(i\gamma W^*) \end{pmatrix}, \qquad \text{(A.6)}$$

where

$$W^* = \int_{z_1}^{z_2} \sqrt{q(z)}dz.$$

Finally, for the solutions in the classically forbidden regions $X < X_1$ and $X > X_2$, the connection matrix is the direct matrix product of the above matrices,

$$\hat{M} = \hat{M}^+ \hat{L} \hat{M}^-.$$

To generalize the procedure to second-order turning points, we must find the connection matrices relating the basic solutions to the Weber equation, namely

$$(\circ, z) \equiv (z)^\nu \exp\left(-\frac{z^2}{4}\right), \qquad \text{(A.7)}$$

and

$$(z, \circ) \equiv (z)^{-\nu-1} \exp\left(\frac{z^2}{4}\right). \qquad \text{(A.8)}$$

In this case, we have four Stokes lines, four anti-Stokes lines, and one cut, and therefore, nine different regions where the solutions must be matched (see Fig. 10a as an illustration). Four Stokes constants are given by

$$\tilde{T}_1 = \tilde{T}_2^{-1}[\exp(i2\pi\nu) - 1], \quad \tilde{T}_3 = \tilde{T}_1^*,$$

$$\tilde{T}_4 = -\tilde{T}_2 \exp(-i2\pi\nu).$$

From the known asymptotic form of the parabolic cylinder functions, we can obtain the remaining Stokes constant

$$\tilde{T}_2 = \frac{\sqrt{2\pi}}{\Gamma(-\nu)}.$$

The connection matrix for an isolated second-order turning point can therefore be represented as

$$\begin{pmatrix} -\tilde{T}_2 & \cos(\pi\nu) \\ \cos(\pi\nu) & -\dfrac{\sin^2(\pi\nu)}{\tilde{T}_2} \end{pmatrix}. \qquad \text{(A.9)}$$

This matrix depending on the energy ϵ determines, e.g., the instanton semiclassical solutions for the harmonic oscillator, $\epsilon = \nu + 1/2$. It can be verified by explicit calculations that for the harmonic oscillator, the connection matrix also has the same form (A.9) in the WKB approach. The difference could appear only from anharmonic terms in the potential. But for low-energy states with $\epsilon/\gamma \ll 1$, the anharmonic corrections are small and the instanton and WKB connection matrices coincide up to the second order in these correction terms.

For the symmetric double-well potential, the connection matrix describing the variation of the coefficients at the basic solutions in Eqs. (A.7) and (A.8) between the two second-order turning points X_2^0 and X_3^0 is given by

$$\begin{pmatrix} \dfrac{n!}{\sqrt{2\pi}}\left(\dfrac{\Omega_0\gamma}{\Omega_*}\right)^{-\nu+1/2}\exp(\gamma W_E^*) & 0 \\ 0 & \dfrac{\sqrt{2\pi}}{n!}\left(\dfrac{\Omega_0\gamma}{\Omega_*}\right)^{\nu+1/2}\exp(-\gamma W_E^*) \end{pmatrix}, \tag{A.10}$$

where the instanton action is

$$W_E^* = \int_{X_2^0}^{X_3^0} \sqrt{2(V(X) - \frac{\epsilon}{\gamma}}dX \tag{A.11}$$

and Ω_* is the characteristic «oscillation» frequency in the barrier (i.e., in the classically forbidden region). The connection matrix in Eq. (A.10) must be compared with a similar matrix in Eq. (A.6) for two linear turning points. For the asymmetric double-well potential in the region between the second-order and the linear turning points, the matrix analogous to (A.10) is

$$\begin{pmatrix} \left(\dfrac{n!}{\sqrt{2\pi}}\right)^{1/2}\left(\dfrac{\Omega_0\gamma}{\Omega_*}\right)^{-(1/2)(\nu+1/2)}\exp(\gamma W_E^*) & 0 \\ 0 & \left(\dfrac{\sqrt{2\pi}}{n!}\right)^{1/2}\left(\dfrac{\Omega_0\gamma}{\Omega_*}\right)^{(1/2)(\nu+1/2)}\exp(-\gamma W_E^*) \end{pmatrix}. \tag{A.12}$$

All the above matrices allow us to find any other connection matrix that we need in the particular examples considered in the main text of the paper. Any of them can be constructed as a corresponding product of the matrices in (A.4), (A.5), (A.6), (A.9), (A.10), and (A.12). It is worth noting a general property of the connection matrices that the connection matrix is real-valued for all bound states, and off-diagonal elements of the connection matrix are complex for continuum spectrum states.

Similarly to the problem of tunneling through the potential barrier $V(X) = -(1/2)X^2$, all the Stokes and anti-Stokes lines are rotated by the angle $\pi/4$ (see Fig. 10*b*) with respect to the corresponding lines for the parabolic well ($V(X) = (1/2)X^2$ considered above, see Fig. 10*a*). The connection matrix for the tunneling through the barrier is given by

$$\begin{pmatrix} S_1 & -i\exp\left(\dfrac{\pi\alpha}{2}\right) \\ i\exp\left(\dfrac{\pi\alpha}{2}\right) & S_1^{-1}\left(\exp(\pi\alpha)+1\right) \end{pmatrix}, \tag{A.13}$$

where $\alpha = i(2\nu+1)$ and S_1 is the Stokes constant on the first quadrant bisectrix (see Fig. 10*b*). To find the Stokes constant S_1, we must match the sum of the incident and of the reflected waves to the solutions of the Weber equation at $X \to -\infty$ and to the transmitted wave as $X \to \infty$. This gives

$$S_1 = \frac{\sqrt{2\pi}}{\Gamma[(1+i\alpha)/2]}\exp\left(\frac{\pi\alpha}{4}\right).$$

REFERENCES

1. L. D. Landau and E. M. Lifshits, *Quantum Mechanics (non-relativistic theory)*, Pergamon Press, New York (1965).
2. J. Heading, *An Introduction to Phase-Integral Methods*, Wiley-Interscience, London (1962).
3. V. L. Pokrovskii and I. M. Khalatnikov, JETP **13**, 1207 (1961).
4. N. T. Maintra and E. J. Heller, Phys. Rev. A **54**, 4763 (1996).
5. C. S. Park and M. C. Jeong, Phys. Rev. A **58**, 3443 (1998).
6. A. K. Roy, N. Gupta, and D. M. Deb, Phys. Rev. A **65**, 012109 (2002).
7. A. M. Polyakov, Nucl. Phys. B **129**, 429 (1977).
8. S. Coleman, *Aspects of Symmetry*, Cambridge Univ. Press, Cambridge (1985).
9. V. A. Benderskii, D. E. Makarov, and C. A. Wight, *Chemical Dynamics at Low Temperatures*, Willey-Interscience, New York (1994).

10. V. A. Benderskii, E. V. Vetoshkin, and H. P. Trommsdorf, Chem. Phys. **244**, 273 (1999).

11. V. A. Benderskii and E. V. Vetoshkin, Chem. Phys. **257**, 203 (2000).

12. V. A. Benderskii, E. V. Vetoshkin, L. S. Irgebaeva, and H. P. Trommsdorff, Chem. Phys. **262**, 369 (2000).

13. I. M. Lifhsits and Yu. Kagan, JETP **35**, 206 (1972).

14. M. Grifoni and P. Hanggi, Phys. Rep. **304**, 229 (1998).

15. J. E. Avron and E. Gordon, Phys. Rev. A **62**, 062504 (2000).

16. J. Ankerhold and H. Grabert, Europhys. Lett. **47**, 285 (1999).

17. Y. Kaganuma and Y. Mizumoto, Phys. Rev. A **62**, 061401(R) (2000).

18. V. A. Benderskii and E. I. Kats, Phys. Rev. E **65**, 036217 (2002).

19. V. V. Avilov and S. V. Iordanskii, JETP **69**, 1338 (1975).

20. V. A. Benderskii, E. V. Vetoshkin, L. von Laue, and H. P. Trommsdorff, Chem. Phys. **219**, 143 (1997).

21. A. M. Dykhne, JETP **14**, 941 (1961).

22. A. Erdelyi, W. Magnus, F. Oberhettinger, and F. G. Tricomi, *Higher Transcendental Functions*, McGraw Hill, New York (1953), Vol. 1–3.

23. M. Berry, Proc. Roy. Soc. London, ser. A **392**, 45 (1984).

24. M. Wilkinson, J. Phys. A **17**, 3459 (1984).

25. H. Karatsuji, Progr. Theor. Phys. **74**, 439 (1985).

26. A. O. Caldeira and A. J. Legget, Ann. Phys. **149**, 374 (1983).

27. D. Bohm, *Quantum Theory*, Englewood Clifs, New Jersey (1951).

28. L. L. Chang, L. Esaki, and R. Tsu, Appl. Phys. Lett. **24**, 593 (1974).

29. J. P. Eisenstein, L. N. Pfeiffer, and K. W. West, Phys. Rev. Lett. **74**, 1419 (1995).

30. Sh. Matsumoto and M. Yoshimura, Phys. Rev. A **63**, 012104 (2000).

31. M. Baer, Phys. Rep. **358**, 75 (2002).

32. H. Pu, W. Zhang, and P. Meystre, Phys. Rev. Lett. **87**, 140405 (2001).